ELSEVIER

International Journal of Mass Spectrometry 176 (1998) 177–188

International Journal of Mass Spectrometry

Selected ion flow drift tube study of the formation and dissociation of $CO^+.N_2$ ions in nitrogen buffer gas: the $CO^+.N_2$ bond energy

J. Glosík[a,*], G. Bánó[a], E.E. Ferguson[b], W. Lindinger[c]

[a]*Department of Electronics and Vacuum Physics, Mathematics and Physics Faculty, Charles University, V Holešovičkách 2, Prague 8, Czech Republic*

[b]*NOAA-CMDL, 325 Broadway, Boulder, CO 80303, USA*

[c]*Institut für Ionenphysik der Universität Innsbruck, Technikerstrasse 25, Innsbruck, Austria*

Received 11 December 1997; accepted 16 March 1998

Abstract

Efficient vibrational quenching of CO^+ ($v = 1$) by N_2 led to the deduction of an unexpectedly strong attractive potential between CO^+ and N_2. This was subsequently confirmed by *ab initio* quantal calculations of the $CO^+.N_2$ bond strength. The bond energy of $CO^+.N_2$ has now been determined in a selected ion flow drift tube, by measuring collisional destruction and formation of $CO^+.N_2$. The bond energy is found to be 0.7 ± 0.2 eV. This is sufficiently large to rationalize the fast vibrational quenching but somewhat less than an *ab initio* value. The large value of $D(CO^+.N_2)$ can unambiguously be explained by resonance interaction between $CO^+.N_2$ and the charge-transfer $CO.N_2^+$ states. (Int J Mass Spectrom 176 (1998) 177–188)

Keywords: Ion/molecule reactions; Selected ion flow drift tube; $CO^+.N_2$ formation; $CO^+.N_2$ dissociation, CO^+N_2 bond energy

1. Introduction

Hamilton et al. [1] observed a very efficient vibrational quenching of $CO^+(v = 1)$ by N_2, $k_q = (1.3 \pm 0.6) \times 10^{-10}$ cm^3 s^{-1} at 300 K. This quenching rate coefficient is much larger than that for the quenching by N_2 of $O_2^+(v = 1)$, $k_q = 1.9 \times 10^{-12}$ cm^3 s^{-1} [2] and $NO^+(v = 1)$, $k_q = 7 \times 10^{-12}$ cm^3 s^{-1} [3]. It is known that a strong correlation exists between the quenching efficiency and the attractive potential, or complex bond strength, between the respective collision partners [4]. The bond energies for $O_2^+.N_2$ and $NO^+.N_2$ are 0.23 and 0.2 eV, respectively [5]. Because the attractive potential is dominated by the charge-induced dipole term, $V(r) \sim e^2\alpha/r^4$, where α is the neutral polarizability, one might have expected a similar weak bond for $CO^+.N_2$. In pursuit of this enigma, a finding of a large three-body association rate constant for CO^+ and N_2, comparable to that for N_2^+ and N_2, where the bond energy is ~1 eV, led to the suggestion that the bond energy, $D(CO^+.N_2)$, might also be as large as 1 eV [6]. Three-body association rate constants depend on the attractive well depth for the same reason as rate coefficients for vibrational quenching. In both cases the collision of

* Corresponding author.

PII S1387-3806(98)14019-8

an ion with a neutral leads to the formation of a transient (orbiting) complex. In the case of association, the complex is stabilized by collision with a third body. In the case of vibrational quenching, vibrational predissociation competes with unimolecular decomposition of the complex [4]. Both processes then have (in a low pressure limit) rates proportional to the transient complex lifetime, which increases with well depth.

This implies a correlation between vibrational quenching and three-body association rate constant, which has been well established and used to determine typical vibrational predissociation lifetimes, because the three-body rate constant yields the transient complex lifetime. Vibrational predissociation lifetimes for $O_2^+(v)$ and $NO^+(v)$ complexes with small neutrals are found to be typically $\sim 10^{-9}$ s [4].

Subsequently Baker and Buckingham [7] determined the $CO^+.N_2$ bond energy to be 0.97 eV in *ab initio* quantal calculations, at the MP3/6-316*//6-316* level.

The present experiment determines the $CO^+.N_2$ bond energy from measurement of the equilibrium constant and its "temperature" dependence for the system

$$CO^+ + N_2 + N_2 \underset{k_2}{\overset{k_3}{\rightleftharpoons}} CO^+.N_2 + N_2 \qquad (1)$$

in a flow drift tube (k_3 is the three-body association rate coefficient, k_2 is the binary reaction rate coefficient of the collision induced dissociation). In a drift tube experiment, the collision energy or "effective temperature," T_{eff}, of the reacting species is characterized by the average kinetic energy in the center-of-mass frame KE_{CM}, where $KE_{CM} = 3/2\ k_B T_{\text{eff}}$ (see Part 2 of the Appendix for more detail).

In the reaction scheme (1) the binary reaction rate coefficient k_2 is used to characterize the dissociation (reverse) process. In order to describe the collision induced dissociation (CID) in a multicollisional system by a binary reaction rate coefficient we can follow the Lindeman-Hinshelwood model for unimolecular reaction [8]. In this model, one assumes that a reactant ion, $CO^+.N_2$ in the present case, becomes energetically excited, "activated," to $(CO^+.N_2)^*$ by collisions with another molecule (N_2) at the expense of collisional energy. The activated $(CO^+.N_2)^*$ can be deactivated in another collision with N_2 or eventually dissociate according to the following equations:

$$CO^+.N_2 + N_2 \underset{k_{\text{deac}}}{\overset{k_{\text{ac}}}{\rightleftharpoons}} (CO^+.N_2)^* + N_2 \qquad (2)$$

$$(CO^+.N_2)^* \overset{k_{\text{dis}}}{\rightarrow} CO^+ + N_2 \qquad (3)$$

Using the steady-state approximation we can write for the reaction rate coefficient of the overall unimolecular dissociation reaction

$$k_{\text{uni}} = k_{\text{ac}}.[N_2].\frac{k_{\text{dis}}}{k_{\text{dis}} + k_{\text{deac}}.[N_2]} \qquad (4)$$

In the low pressure limit $k_{\text{dis}} \gg k_{\text{deac}}.[M]$, $k_{\text{uni}} \approx k_{\text{ac}}.[N_2]$ and the reaction has second-order kinetics with a pressure independent effective binary reaction rate coefficient, $k_2 \approx k_{\text{ac}}$. In this sense, we deal with CID just as with binary reactions, and we use k_2 to stress second-order kinetics of the reaction. On this occasion, we want to emphasize the basic difference between CID in multicollision systems on the one hand, where the internal state distribution of the molecular ions ($CO^+.N_2$ in the present experiment) before activation is determined by some type of "thermal equilibrium" and, on the other hand, CID in single collision experiments, where internal energy of the dissociated ions is usually governed by the ion source conditions.

The validity of using drift tube measurements (where KE_{CM} and/or T_{eff} are used instead of a true temperature) to determine thermochemical quantities is questionable and controversial. There are two basic problems in using average KE_{CM} instead of true temperature. The first one is that ions drifting under the influence of an electric field in a buffer gas do not always have velocity distributions close to Maxwellian, so that strictly speaking a valid translational temperature does not exist. It is known that the diatomic ion velocity distributions in He buffered drift tubes are close to Maxwellian, that there is a high energy tail deviation in Ar buffered drift tubes, and

that N_2 lies in between. The second problem is that internal degrees of freedom are not in equilibrium with the average KE_{CM}. The reactant ions are probably rotationally excited to equilibrium, and the ions are probably not fully vibrationally excited to equilibrium. The rotational and vibrational temperatures of the neutral reactants (N_2) remain at buffer gas temperature (300 K in the present experiment). This subject has been reviewed in some detail by Albritton [9], and other authors. In the scope of the present, mostly experimental, work we cannot fully solve the problem of internal energy distribution in the drift tube experiments.

It is quite clear that situations do occur where drift tubes provide valid thermochemical data. The case closest to the present offers considerable encouragement: CID measurements of $(CO)_2^+$, N_4^+, Kr_2^+, and N_2Ar^+ in helium buffer, taken in the same selected ion flow drift tube (SIFDT) used here, gave linear Arrhenius plots yielding activation energies equal to the known bond energies to within the uncertainties of the known bond energies [10]. For example, Tichy et al. [11] found linear Arrhenius and van't Hoff plots for seven proton transfer reactions and equilibria in which the average difference between the deduced values of ΔH^0 and known proton affinity (PA) differences was 0.36 kcal mol^{-1}, well within the error bars of any PA scale. The average deviations for ΔS^0 were 1 cal mol^{-1} K^{-1} (or $T\Delta S^0 = 0.3$ kcal mol^{-1} at 300 K). By contrast, proton transfer between N_2O and CO gave nonlinear KE_{CM} Arrhenius and van't Hoff plots [12]. Ideally, linear plots would imply at least approximate thermochemical validity and inappropriate circumstances would lead to nonlinear plots. In our Discussion section we give our reasons for believing that those problems do not invalidate the present results but do yield large error bars on our final result to include what we believe the uncertainties to be.

2. Experimental

The experiments were conducted with the Innsbruck SIFDT of a conventional design. N_2 was used as a carrier-buffer gas in the present experiment. The SIFDT has been described in detail many times (see e.g. Villinger et al. [13] and Glosík et al. [14]) and also in our previous papers, where CID of molecular ions drifting in He buffer gas was studied [10,15]. Only a short description of experimental conditions and explanation of data analyses is given here. CO^+ ions were produced from CO by electron impact in a low pressure ion source. The ions were mass selected using a quadrupole mass filter and injected with very low kinetic energy through a Venturi type inlet into the upstream part of the flow-drift tube into flowing neutral N_2 gas. The injection energy of the ions was kept small to eliminate collisional dissociation of CO^+ and formation of N_2^+ ions by charge transfer to N_2 in the first few collisions after injection. The energy of the CO^+ ions further downstream in the drift tube is in the present experiment too small ($KE_{CM} < 0.2$ eV in collision of ions with N_2) for the formation of N_2^+ in the endoergic charge transfer (endoergic by 1.567 eV). Also formation of N_4^+ from $CO^+.N_2$ by a "switching" reaction is endoergic by >1.6 eV. Absence of N_2^+ in the drift tube is critical. Presence of N_2^+ in the drift tube will cause formation of N_4^+ and because of mass coincidence of N_2^+ and N_4^+ with CO^+ and $CO^+.N_2$, respectively, the data analysis will be very difficult if not impossible. Injected CO^+ ions are "thermalized" in the upstream part of the drift tube with relatively weak axial electric field. In the present experiment, the SIFDT was not used in the conventional way, where reaction rate coefficients of ion–molecule reactions are measured by monitoring ionic number densities as a function of an addition of neutral reactant gas.

In the present experimental conditions, the injected CO^+ ions drift along the drift tube and react with N_2 in the three-body association reaction and $CO^+.N_2$ ions are produced. The $CO^+.N_2$ ions can then dissociate back in collisions with N_2. Number densities of the different ions at the end of the drift tube depend on the initial conditions, length of the drift tube, pressure and on E/N (where E is electric field strength and N is neutral N_2 number density) in the drift tube. At a particular pressure and E/N in the drift tube, the relative number densities of CO^+ and $CO^+.N_2$ ions

can be monitored by the downstream mass spectrometer and ion counting system. To obtain rates of the processes taking place in the drift tube, the drift tube is divided into two sections, with different values of E/N. The first, upstream section is used to form certain "initial conditions" at the beginning of the second, downstream section. The actual E/N in the second section is adjusted in a way that the particular processes under study, CID or association, are taking place in the second section of the drift tube. The length of the second section can be varied at the expense of the length of the first section. By changing the length of the second section the reaction time is changed and the time evolution of the ionic composition (corresponding to equilibrium or approach to equilibrium) can be determined. In order to have constant "initial conditions" at the beginning of the second section, independent of actual length of the second section, they have to also be independent of the length of the first section.

Two specific "initial conditions" were used in the present experiment. With high E/N in the first section, association is suppressed and only CO^+ ions are present at the beginning of the second section. With low E/N in the first section, all injected CO^+ ions associate and only $CO^+.N_2$ ions are present at the beginning of the second section. The "low" and "high" values of the E/N at a particular pressure of the buffer gas can be determined by extending the first section to the whole length of the drift tube and monitoring the actual "initial composition" by the downstream mass spectrometer. The actually used "low" E/N is even lower and "high" E/N is even higher to ensure constant initial conditions, 100% association or 100% dissociation, for all used values of the length of the first section of the flow-drift tube. The more detailed description of the data analysis is given in Part 3 of the Appendix. Certain experimental conditions, e.g. maximum voltage on the drift tube, minimum pressure, and so forth, favor measurements with "low" E/N in the first section. Most of the equilibrium constants were determined by producing $CO^+.N_2$ in the first section and its dissociation towards equilibrium in the second section. As is shown in Part 3 of the Appendix, for the length L of the

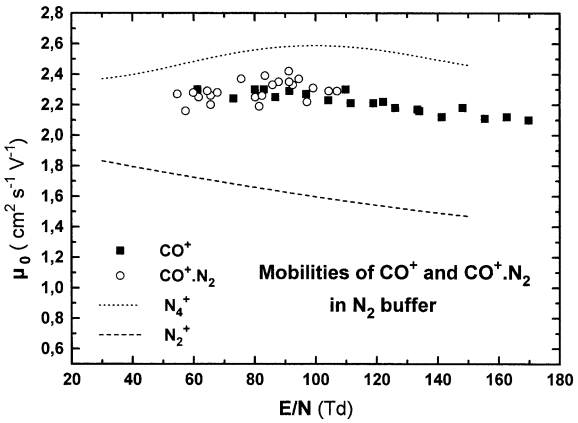

Fig. 1. Reduced mobility of CO^+ (filled square) and $CO^+.N_2$ (open circle) in N_2. Dotted line represents reduced mobility of N_4^+ in N_2 [17]; dashed line represents mobility of N_2^+ in N_2 [16].

second section of the drift tube, the relative concentration $F_{(CO+.N_2)}$ of $CO^+.N_2$ is given by

$$F_{(CO^+.N_2)} = \frac{[CO^+N_2]_t}{[CO^+]_0 + [CO^+N_2]_0} = \frac{K_C[N_2]}{1 + K_C[N_2]}$$

$$- \frac{(K_C[CO^+]_0[N_2] - [CO^+N_2]_0)e^{-k_2(K_C[N_2]+1)}[N_2]^t}{([CO^+]_0 + [CO^+N_2]_0)(K_C[N_2] + 1)} \quad (5)$$

where time $t = L/(v_d + v_{flow})$, and K_C is the equilibrium constant in terms of concentrations (see Part 3 of the Appendix for details). The velocity of the flow of buffer gas, v_{flow}, is calculated from the measured flow rate of N_2 and its pressure. The drift velocity, v_d is calculated at particular E/N and pressure from the mobility μ of the particular ion in N_2. The reduced mobilities, μ_O of CO^+ and $CO^+.N_2$ in N_2 were measured on the same apparatus. Measured reduced mobilities are plotted in Fig. 1. It was not easy to measure mobilities over an extended E/N range because association takes place at low E/N and dissociation at high E/N. Note that the mobilities of both ions are approximately equal at E/N from 60 Td up to 110 Td. This is a very fortunate situation because it implies that at a given E/N the drift velocities of both types of ions are equal. If the drift velocities are equal then also the collisional energies

of both ions with neutral N_2 are the same (see details in Part 2 of the Appendix). This is important when applying a thermodynamical approach to measured data.

When the injection energy of CO^+ was too high, N_2^+ and N_4^+ ions were also observed in the arrival spectra, and because of their different mobilities, it was easy to recognize them and to suppress the presence of N_2^+ ions in the drift tube by decreasing the kinetic energy of the injected ions. Reduced mobilities of both N_2^+ [16] and N_4^+ [17] in N_2 are also included in Fig. 1 to demonstrate the difference from the reduced mobilities of CO^+ and $CO^+.N_2$ in N_2. Positions of "additional maxima" in an arrival spectrum were in good agreement with corresponding mobilities of N_2^+ and N_4^+ ions. For higher E/N, where we did not obtain mobilities of $CO^+.N_2$ by direct measurement, values obtained by short extrapolation (not exceeding 130 Td) were used for the calculation of v_d and KE_{CM}.

Special care was paid to the tuning of the detector mass spectrometer to reduce mass discrimination, because that can change the deduced relative composition of the ions and influence the determination of the value of the function $F_{(CO^+.N_2)}$. By changing the length of the second section of the drift tube, i.e. by changing the composition of the ions at the front of the detector system, we did not observe a significant change in the total number of counts in the detector, indicating that a mass discrimination is small and can be neglected in our analyses.

In Fig. 2, the relative concentration of $CO^+.N_2$ versus length L of the second section of the drift tube [function $F_{(CO^+.N_2)}(L)$], obtained from data measured at 0.17 Torr, is plotted for different KE_{CM}. "Low" E/N, i.e. nearly 100% association in the first section, was used in these measurements, as can be seen from $F_{(CO^+.N_2)}(L = 0) \approx 1$. Lines represent the best fit. Small shift of the intersection from $L = 0$ can be explained by the finite length of the segment of the drift tube (2.16 cm) and by inhomogeneity of the electric field between sections. The shift indicates the maximum length (or corresponding number of collisions with N_2) in which steady-state conditions, characterized by constant effective temperature (T_{eff}) and

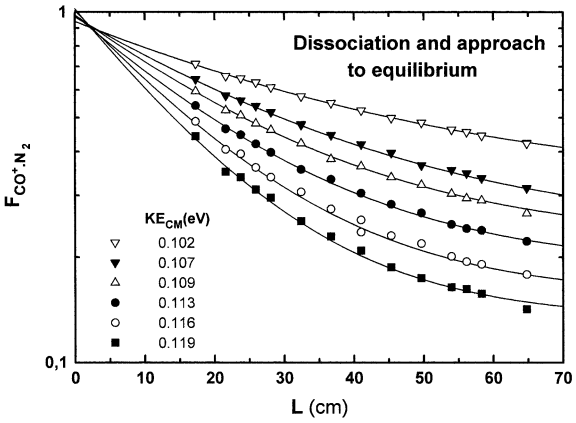

Fig. 2. Evolution of the relative concentration of $CO^+.N_2$ along the second section of the drift tube at 0.17 Torr. Length (L) is the distance between the downstream end of the drift tube and the actual beginning of the second section. Different KE_{CM} are indicated by the different symbols. The lines represents the best fit of the data by function $F_{CO^+.N_2}(L)$; the resulting k_2, k_3, and K_P values are plotted in Figs. 4, 5, and 6, respectively.

constant k_2 and k_3, are reached. By fit of the data with function $F_{(CO^+.N_2)}(L)$ the parameters K_C and k_2 were obtained. In Fig. 3, the relative concentration of CO^+ [function $F_{CO^+}(L)$] is plotted for different, near-thermal KE_{CM}. The relative concentration of the produced $CO^+.N_2$ ions is also plotted. The maximum possible voltage on the drift tube limited the maximum degree of the dissociation in the first section to 70%. The equilibrium for this set of the measurements occurs at very low relative concentration of CO^+ and high relative concentration of $CO^+.N_2$, so the equilibrium constants cannot be determined accurately and only k_3 can be determined. Such experimental conditions were adjusted deliberately to determine an accurate value of the three-body association rate coefficient in N_2 at near-thermal energies.

3. Results

Fig. 4(a) gives the measured binary break-up rate constant k_2 versus KE_{CM} and Fig. 4(b) gives the resulting Arrhenius plot. k_2 was measured in the pressure range from 0.14 to 0.27 Torr and no pressure dependence was observed, indicating that the process

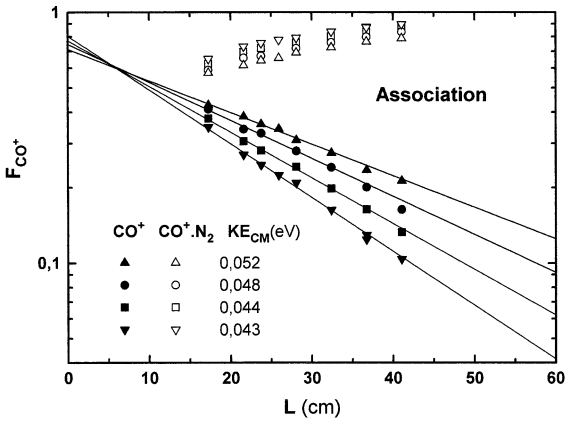

Fig. 3. Evolution of the relative concentrations of primary CO^+ (filled symbols) and product $CO^+.N_2$ (open symbols) ions along the second section of the drift tube at 0.17 Torr. L is the distance between the downstream end of the drift tube and the actual beginning of the second section. Different, near thermal, KE_{CM} are indicated by the different symbols. The lines represents the best fit of the data by the function $F_{CO^+}(L)$; resulting k_3 are plotted in Fig. 5. K_P was not determined from these measurements because the system is governed by dissociation and the influence of the reverse process is negligible; equilibrium will be reached only at very high L and low $[CO^+]$.

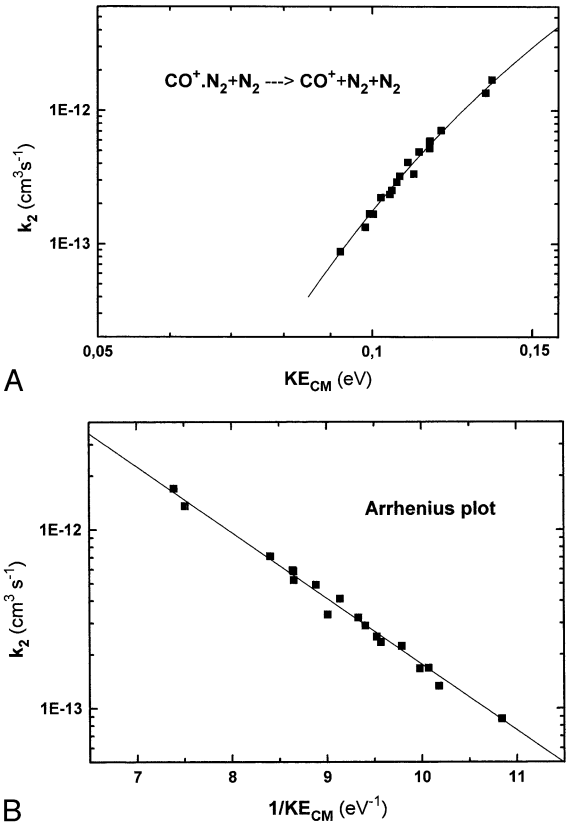

Fig. 4. (a) Energy (KE_{CM}) dependence of the rate coefficient k_2 of the CID of $CO^+.N_2$ drifting in N_2. The rate coefficients k_2 were obtained by fit of the "approach to equilibrium from 100% association" using function $F_{(CO^+.N_2)}(L)$. The measurements were carried out in the pressure range of 0.14–0.27 Torr and no pressure dependence of k_2 was observed. The data (k_2) were fitted by the Arrhenius formula (full line); resulting parameters of the fit: Arrhenius activation energy $E_a = 0.57$ eV and Arrhenius pre-exponential factor $A = 8.6 \times 10^{-10}$ cm^3 s^{-1} (corresponding Langevin collision rate coefficient for collision of $CO^+.N_2$ with N_2, $k_L = 7.1 \times 10^{-10}$ cm^3 s^{-1}). (b) Arrhenius plot of the rate coefficient k_2 of the CID of $CO^+.N_2$ drifting in N_2; data taken from (a).

has second-order kinetics, as was already discussed. The straight line in Fig. 4(b) gives $k_2 = 8.6 \times 10^{-10}$ exp(-0.57 eV/k_BT_{eff})cm^3 s^{-1}, where k_BT_{eff} is given in [eV] and $k_BT_{\text{eff}} = 2/3\text{KE}_{\text{CM}}$. The obtained Arrhenius activation energy $E_a = 0.57$ eV. Note that the preexponential factor is close to the Langevin collision rate constant for collision of $CO^+.N_2$ with N_2, $k_L = 7.1 \times 10^{-10}$ cm^3 s^{-1}. This may indicate that the activation process is very effective [see Eqs. (2), (3), and (4)] and activation is taking place at every energetically allowed collision. Nevertheless, we have to keep in mind that the real process is multilevel and multicollisional.

Fig. 5 shows the three-body association rate constant, k_3, as a function of KE_{CM}. There are two sets of data plotted in Fig. 5: at low KE_{CM} (closed circles), the data obtained by direct measurements of the rate of the association. It was possible to measure k_3 only at near thermal energies ($T_{\text{eff}} \sim 300$ K) because a sufficient electric field to produce complete dissociation in the first drift region was not attainable and the resulting CO^+ concentrations did not sensitively measure k_3. At higher KE_{CM} are plotted the data (open circles) calculated from the measured equilibrium constant, K_C, and the measured rate coefficient of the reverse process, k_2, of CID of $CO^+.N_2$ (for details see Appendix). As a function of $3/2k_BT$ shown are the values measured in a temperature variable system (VT-SIFT) at 80 K and 300 K with He third body [6]. Extrapolation of the drift tube data (dotted line) to KE_{CM} corresponding to 300 K gives k_3 (300 K) =

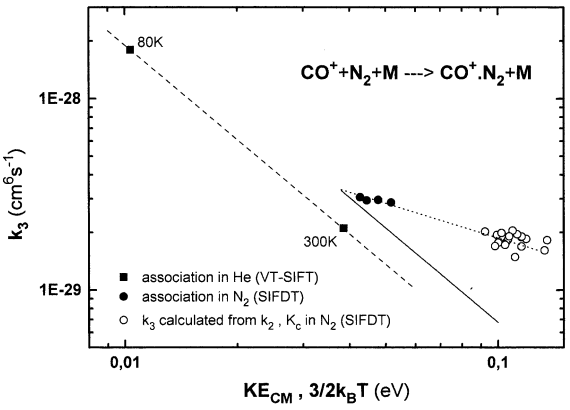

Fig. 5. Three-body association reaction rate coefficient k_3 of the association of CO^+ with N_2. Filled squares indicate thermal data as obtained by Ferguson et al. [6] in He buffer in a VT-SIFT experiment. Filled circles indicate near thermal data (N_2 buffer) obtained in the present experiment (see Fig. 3). Note that at 300 K, N_2 is nearly two times more efficient than He in the stabilization of the collision complex. Open circles indicate association rate coefficients (in N_2) calculated from the dissociation rate coefficients k_2 and the equilibrium constants K_C obtained by fits of the "approach to equilibrium from 100% association" using function $F_{(CO+.N_2)}(L)$; see Figs. 4 and 6. The full line indicates the expected "thermal" association rate coefficient in N_2 if the same temperature dependence is assumed as was observed in the thermal study in He buffer, and the increase of the stabilization efficiency is taken from the comparison of the present near thermal data and SIFT data [6].

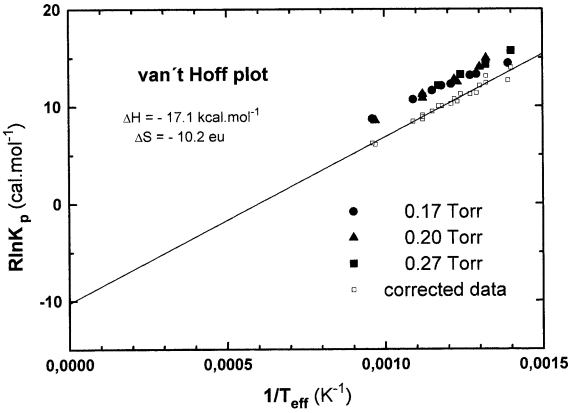

Fig. 6. Plot of the obtained equilibrium constant K_P (filled symbols) and corrected values (open square). Different pressures are indicated by different symbols. Line represents fit of the data by van't Hoff formula, obtained parameters are: $\Delta H_P^0 = -17.1$ kcal mol^{-1}, and $\Delta S_P^0 = -10.2$ cal mol^{-1} K^{-1}.

3×10^{-29} cm^6 s^{-1}. As expected, the obtained k_3 (300 K) for the association rate coefficient with N_2 as a third body is larger than the corresponding value for He as the third body.

The dependence of k_3 (dotted line) on KE_{CM} is not appropriate for use in thermodynamic relations because in the three-body association in a real thermal system, the increasing rotational energy of the neutral N_2 with T inhibits association. All internal energy decreases the lifetime of transient complexes. The applied electrical field does not increase the neutral rotational energy and thus underestimates the T dependence of measured k_3; the slope of the dotted line is smaller than the slope of the dashed line. When E/N approaches zero, KE_{CM} approaches thermal energy, and the measured k_3 approaches the real thermal value at 300 K. We assume the measured 300 K value of k_3 (300 K) is correct and in addition we assume that the correct T dependence is given by the true temperature data [6], so that the correct dependence of k_3 is represented by the solid line in Fig. 5. The dependence obtained is $k_3 \sim T^{-1.6}$. The actual "empirical" correction represents in very good approximation multiplication by the factor T^{-1}. Following previous work by Bates it was deduced by Adams and Smith [18] that $k_3 \approx 1/T_n^{r/2}$, where T_n and r are the temperature and number of rotational degrees of freedom of reactant neutral, respectively (see also discussion and experimental data in Glosík et al. [19]). From this dependence it follows, that in the case of the reaction of N_2, the k_3 obtained in a drift experiment will differ from the k_3 obtained in a temperature variable system by the factor T^{-1}, which is in excellent agreement with the actual correction, i.e. the ratio between dotted and solid lines.

Because $K_C = k_3/k_2$, K_C will suffer the same defect just described and will accordingly need to be corrected with, as we shall see, a relatively small correction (corresponding changes of ΔH^0 and ΔS^0 are -0.09 eV and -4.1 cal mol^{-1} K^{-1}, respectively.) The K_C values measured at different pressures are converted to K_P and plotted in Fig. 6 in the form of a van't Hoff plot, $R \ln K_P$ versus T_{eff}^{-1}, and the data are denoted by closed symbols. The open symbols are the corrected data. This plot yields $\Delta H^0 = -0.74$ eV from the slope and $\Delta S^0 = -10.2$ cal mol^{-1} K^{-1}. If

the above correction to the energy dependence were not made, ΔH^0 would increase to -0.65 eV and ΔS^0 to -6.1 cal mol^{-1} K^{-1}.

The difference between E_a from the Arrhenius plot and ΔH^0 from the van't Hoff plot follows from the negative T dependence of three-body association, equivalent to a negative activation energy, E_b. $\Delta H^0 \approx \Delta E = -(E_a - E_b)$ follows from $K = k_3/k_2$ (see Appendix, Part 3). The ratio of k_3 between 700 and 1000 K, the range of the van't Hoff plot (Fig. 6), is $(1000/700)^{-1.6}$. The activation energy that would give the same ratio for these two temperatures from $k_3 \sim \exp(-E_b/k_BT)$ is $E_b = -0.125$ eV. Thus, $\Delta E = -(0.57 + 0.125)$ eV $= -0.695$ eV, similar to the value of ΔH^0 deduced from the van't Hoff plot. Of course an exponential does not fit k_3 as well as a T^{-n} plot, which is a way of saying the activation energy is not really a constant, but this shows that the difference between ΔH^0 and E_a has a plausible value.

We also believe that it is plausible that the presence or absence of buffer gas N_2 rotational energy does not significantly influence collisional breakup, just from the mechanistic viewpoint. The rotational energy is small compared with the energy necessary to be transferred and can have little if any influence on the energy transfer. The energies involved in the range of the van't Hoff plot (0.09–0.14 eV) are small compared with CO^+ or N_2 vibrational energies; this vibration thus does not come into play.

Fig. 7 compares the present $CO^+.N_2$ breakup van't Hoff plot along with earlier plots for N_4^+ and $O_2^+.N_2$, clearly showing that the $CO^+.N_2$ bond is much larger in energy than that of $O_2^+.N_2$, 0.22–0.25 eV [5] and somewhat less than that of N_4^+, 0.9–1.1 eV [5].

The entropy change from association is largely due to loss of the three translational degrees of freedom of the one less particle but is offset somewhat by the very low frequency bending modes of the weak complex and its very low rotational constant. The 10 eu entropy change is not nearly precise enough (because of the long extrapolation) to use in determining vibrational or rotational constant data.

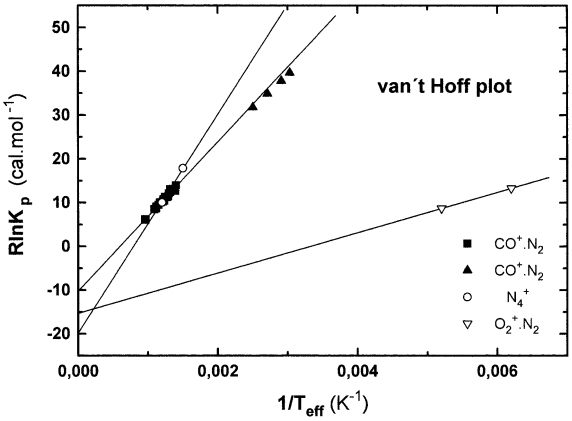

Fig. 7. Extended van't Hoff plot of the equilibrium constant. Filled squares indicate present SIFDT data (identical with corrected date plotted in Fig. 6); filled triangles indicate "thermal data" calculated of thermal k_3 [measured and corrected $k_{3\text{CORRECTED}} = k_{3\text{MEASURED}}.(T/300)^{-1}$] and k_2 (obtained by extrapolation of measured data, see Fig. 4(b)). For the comparison also included are samples of the data obtained by Hiraoka and Nakajima [26] in their high pressure mass spectrometer for cluster ions $O_2^+.N_2$ (open reverse triangles) and $N_2^+.N_2$ (open circles); lines crossing these data are given by respective ΔH_P^0, and ΔS_P^0 in the corresponding clustering reactions.

4. Discussion

The present finding, $D(CO^+.N_2) = 0.7 \pm 0.2$ eV, confirms the qualitative estimate of a strong bond, relative to $NO^+.N_2$ or $O_2^+.N_2$ bonds, which have a bond energy of ~0.2 eV. This value is somewhat less than the *ab initio* value of 0.97 eV.

The present value can be rationalized as follows. The essence of the matter is recognition of the role of resonance interaction between the ground state $CO^+.N_2$ and the charge-transfer state $CO.N_2^+$. Such an analysis was carried out for a number of O_2^+ and NO^+ clusters with small neutrals [20] in which it was shown that the charge-transfer contribution to bonding, there called *incremental bond energy*, is generally quite significant. Determining an empirical interaction matrix element, H_{12}, equal to 0.7 eV for O_2^+ cluster and 0.95 eV for NO^+ cluster by least squares fit to the data, gave an excellent correlation between calculated and experimental bond energies.

This model divides the attractive force into a purely classical electrostatic attraction dominated by

the charge-induced dipole term, $V(r) \sim e^2\alpha/r^4$, and a quantum mechanical term resulting from resonance attraction of the two interacting states.

We estimate the resonance interaction in two ways. Pauling [21] provides a curve of effective resonance energy as a function of the difference in energy of the two interacting states. In this case, that is the difference in IPs of N_2 and CO, 1.567 eV. The energy is scaled by the interaction matrix element H_{12} and the curve is the solution of the secular equation for two interacting states. We take H_{12} to be equal to ~1 eV, corresponding approximately to the bond energy for $N_2^+.N_2$ or $CO^+.CO$. The matrix element H_{12} reflects the wave function overlap for the charge-transfer donor and acceptor orbitals. For N_2 and N_2^+ these are $\sigma_g 2p$ orbitals, which have good overlap for a linear N_4^+ complex. The isoelectronic CO and CO^+ will have similar orbitals (although the center of symmetry is lost); hence, the similar bond energies for $N_2^+.N_2$ and $CO^+.CO$. From Pauling's curve (or the analysis of Gislason and Ferguson [20]), the effective resonance energy for an energy difference of ~1.5 times H_{12} is $\sim 1/2H_{12}$ or ~0.5 eV.

The importance of charge-transfer is clearly established by the *ab initio* calculation. Baker and Buckingham [7] find that 20–30% of the charge on $CO^+.N_2$ resides on the N atoms, the amount depending on which of four schemes for partitioning charge that they used: 20% (Mulliken), 29% (Löwdin), 24% (distributed multipole analysis), or 22% (natural population analysis). This charge distribution can be used to calculate the interaction stabilization using the Mulliken charge-transfer theory [22]. The wave function is written by Mulliken as $\Psi = a\Psi_{NB} + b\Psi_D$, where Ψ_{NB} is the state without charge transfer and Ψ_D is the charge-transfer (dative) state. The dative coefficient b^2 ranges from 20% to 30%. The stabilization energy E_- is $b^2\Delta E$, where ΔE is the energy difference in the two states, 1.567 eV. Thus, E_- ranges from 0.31 to 0.47 eV, depending on the value of b^2 adopted. Adding this stabilization energy to ~0.2 eV electrostatic bonding energy gives $D(CO^+.N_2)$ values from 0.51 to 0.67 eV, again in qualitative agreement with the present experiment. There can be no question that the essential nature of $CO^+.N_2$ bonding is about one-third electrostatic and about two-thirds resonance interaction. This is just what Baker and Buckingham deduced, although they called the exchange energy an "inductive effect." Their total energy, $D(CO^+.N_2) = 0.97$ eV, seems to be too large in our opinion, because from the resonance exchange model it must be less than $D(N_2^+.N_2)$ and $D(CO^+.CO)$, both ~1 eV, unless the wave function overlap is greater for $CO^+.N_2$, which seems unlikely in view of the isoelectronic nature of CO and N_2.

The uncertainty associated with the applications of drift tubes to thermochemistry, discussed in the Introduction, specifically the deviation of the ion velocity distribution from Maxwellian and the nonequilibration of the neutral vibrational temperature from T_{eff}, leads to a large uncertainty in the true break-up rate constant k_2 and hence in $D(CO^+.N_2)$. We believe an estimation uncertainty of ±0.2 eV is generous and that 0.7 ± 0.2 eV encompasses the true value. One point is that a very linear Arrhenius plot (Fig. 4(b)) is obtained. Because both of the above sources of error would be energy dependent, it seems unlikely that large contributions of these effects would yield a linear plot. The presumed occurrence of a high energy velocity distribution tail implies a measured value of k_2 too large, i.e. larger than would be the case for a true Maxwellian distribution without the tail. By contrast, the failure of the neutral N_2 to be vibrationally excited implies a value of k_2 too small, because the N_2 vibration that would exist at a true $T = T_{\text{eff}}$ could only assist the break-up and thus lead to a larger k_2.

The precise value of $D(CO^+.N_2)$ is not of great importance. It is clear that it greatly exceeds $D(O_2^+.N_2)$ and $D(NO^+.N_2)$ and this rationalizes the much faster vibrational quenching of $CO^+(v)$ than $O_2^+(v)$ or $NO^+(v)$ by N_2. It is also clear that $D(CO^+.N_2)$ is somewhat less than $D(N_2^+.N_2)$ and thus somewhat less than predicted by previous *ab initio* theory. It is probable that a precise value of $D(CO^+.N_2)$ is only attainable by more precise *ab initio* theoretical calculations, at a level now possible, and which will, it is hoped, be carried out. The present results and analysis clearly establish the origin of

relatively large $D(CO^+.N_2)$, previously thought to be anomalous, as being due to charge-transfer stabilization from CO^+ to N_2 in the complex.

Acknowledgements

G.B. is thankful to Österreichischer Akademischer Austauschdienst for a scholarship that allowed his stay at Institut für Ionenphysik, Universität Innsbruck. J.G., G.B., and E.E.F. wish to express their thankfulness for the hospitality during their visit at the Institut für Ionenphysik. This work was supported in part by the Fonds zur Förderung der Wissenschaftlichen Forschung under project No. 10014, and in part by Charles University Prague under project No. GA UK 179/1996. Cooperation of Czech and Austrian partners took place within the frame of project ACTION No. 10p3.

Appendix

1. Drift and diffusion

As already mentioned, the reduced mobilities of CO^+ and $CO^+.N_2$ in N_2 are approximately equal at the E/N applied in the present experiment (Fig. 1). From the generalized Einstein relation between mobility and diffusion coefficient [16], it follows that also diffusion coefficients of both ions in N_2 are approximately equal at the E/N applied in the present experiment. Because the diffusion coefficients are comparable, the diffusion losses along the drift tube do not change the relative population of the ions in the drift tube, that is changed only by reactive processes (association and dissociation) in the drift tube. A more concise analysis (given for similar experimental conditions in Glosík et al. [10]) reveals that diffusion losses in the present experimental conditions are small and their influence on ionic composition can be neglected because the difference between the respective values of mobilities are significantly smaller than their absolute values. Because the diffusion losses change only absolute values and not relative values of the number densities of the ions "diffusion terms" are not included in the analysis.

2. Collision energies in a drift tube

We consider an association reaction

$$A^+ + B + M \rightleftharpoons AB^+ + M \tag{6}$$

where M is buffer gas atom (molecule). Several different types of collisions are taking place in a drift tube in such a case: A^+ with B, A^+ with M, AB^+ with M, and so on. Because of the different relative velocities and reduced masses in these collisions, particular collisions are characterized by different average kinetic energies in the center-of-mass frame, KE_{CM} [23]. We denote these energies as $KE_{CM}(A^+;B)$, $KE_{CM}(A^+;M)$, $KE_{CM}(AB^+;M)$, and so on. All these energies are dependent on E/N, which is "the proper parameter" to characterize the collision energies taking place in the system. $KE_{CM}(A^+;B)$ is usually used to characterize kinetic energy dependence of the reaction of ion A^+ with neutral particle B. By using different buffer gases in drift tube experiments, it was demonstrated for several reaction systems that $KE_{CM}(A^+;M)$ is influencing the internal energy of the drifting ions. Often several effective temperatures are used to describe equilibrium (not thermodynamic equilibrium) in such systems. The simplification in the present experiment is that the reactant gas and buffer gas are the same, and fortunately the mobilities of CO^+ in N_2 and $CO^+.N_2$ in N_2 are equal (in the considered E/N range). This implies that the drift velocities $v_d(CO^+;N_2)$ of CO^+ and $v_d(CO^+.N_2;N_2)$ of $CO^+.N_2$ are equal, and consequently $KE_{CM}(CO^+;N_2) = KE_{CM}(CO^+.N_2;N_2)$. Because of this, we are using in the text simply KE_{CM} instead of distinguishing between $KE_{CM}(CO^+;N_2)$ and $KE_{CM}(CO^+.N_2;N_2)$. As effective temperature in this context we use T_{eff} given by the formula: $KE_{CM} = 3/2k_BT_{eff}$.

3. Approach to equilibrium

We consider the reaction

$$A^+ + B + B \underset{k_2}{\overset{k_3}{\rightleftharpoons}} AB^+ + B \tag{7}$$

in which both forward (three-body association, with rate coefficient k_3 and with product AB^+) and reverse (binary collision induced dissociation, with rate coefficient k_2) reactions are important and cannot be neglected at given experimental conditions. The rate of change of $[A^+]$ has two contributions: it is depleted by the forward reaction at a rate $k_3.[A^+][B][B]$ but it is replenished by the reverse reaction at a rate $k_2.[AB^+][B]$. The net rate of change is therefore

$$\frac{d[A^+]}{dt} = -k_3[A^+][B][B] + k_2[AB^+][B] \tag{8}$$

If the initial concentration of A^+ is $[A^+]_0$ and the initial concentration of AB^+ is $[AB^+]_0$, at all times $[A^+] + [AB^+] = [A^+]_0 + [AB^+]_0$ (if diffusion is neglected as was discussed above),

$$\frac{d[A^+]}{dt} = -(k_3[B] + k_2)[A^+][B] + k_2([A^+]_0 + [AB^+]_0)[B] \tag{9}$$

The solution of this first-order differential equation, with the initial conditions $[A^+]_{t=0} = [A^+]_0$ and $[AB^+]_{t=0} = [AB^+]_0$ is

$$[A^+]_t = \frac{([A^+]_0 + [AB^+]_0)k_2 + (k_3[A^+]_0[B] - k_2[AB^+]_0)e^{-(k_3[B]+k_2)[B]t}}{k_3[B] + k_2} \tag{10}$$

If a system is in thermodynamic equilibrium, then the time derivative on the left side of Eq. (8) is $d[A^+]/dt = 0$ and $k_3/k_2 = [AB^+]_{eq}/[A^+]_{eq}[B]_{eq}$. If the equilibrium constant $K_C = \{[AB^+]_{eq}/[A^+]_{eq}[B]_{eq}\}$ is introduced, then

$$\frac{[AB^+]_{eq}}{[A^+]_{eq}[B]_{eq}} = K_C = \frac{k_3}{k_2} \tag{11}$$

(for details see e.g. Atkins [24] and Smith [25]). The relation between K_C, k_3, and k_2 is used in the text to calculate k_3 from measured values of K_C and k_2. Using relation (11) we can construct the function:

$$F_{A^+} = \frac{[A^+]_t}{[A^+]_0 + [AB^+]_0} = \frac{1}{1 + K_C[B]} + \frac{(K_C[A^+]_0[B] - [AB^+]_0)e^{-k_3[B](1+1/K_C[B])[B]t}}{([A^+]_0 + [AB^+]_0)(K_C[B] + 1)} \tag{12}$$

and similarly for $[AB^+]_t$:

$$F_{AB^+} = \frac{[AB^+]_t}{[A^+]_0 + [AB^+]_0} = \frac{K_C[B]}{1 + K_C[B]} - \frac{(K_C[A^+]_0[B] - [AB^+]_0)e^{-k_2(K_C[B]+1)[B]t}}{([A^+]_0 + [AB^+]_0)(K_C[B] + 1)} \tag{13}$$

The second terms with the exponential in both equations represent approach to equilibrium. When time approaches infinity, $t = \infty$, the concentrations reach their equilibrium values:

$$\frac{[A^+]_\infty}{[A^+]_0 + [AB^+]_0} = \frac{1}{1 + K_C[B]} \tag{14}$$

and similarly for $[AB^+]_t$:

$$\frac{[AB^+]_\infty}{[A^+]_0 + [AB^+]_0} = \frac{K_C[B]}{1 + K_C[B]} \tag{15}$$

Both Eqs. (12) and (13) can be used to determine k_2 and k_3; the accuracy of the determination depends on the value of $K_C[B]$. For $K_C[B] \ll 1$ and $[A^+]_0 \leq [AB^+]_0$ the determination of k_2 is more accurate; for $K_C[B] \gg 1$ and $[A^+]_0 \geq [AB^+]_0$, the determination of k_3 is more accurate. The reaction time is determined from the velocity of the ions, given by flow and drift velocities, and from the length of the second section of the drift tube.

References

[1] C.E. Hamilton, V.M. Bierbaum, S.R. Leone, J. Chem. Phys. 83 (1985) 601.
[2] H. Böhringer, M. Durup-Ferguson, D.W. Fahey, F.C. Fehsenfeld, E.E. Ferguson, J. Chem. Phys. 79 (1983) 4201.

[3] W. Federer, W. Dobler, F. Howorka, W. Lindinger, M. Durup-Ferguson, E.E. Ferguson, J. Chem. Phys. 83 (1985) 38.
[4] E.E. Ferguson, J. Phys. Chem. 90 (1986) 731.
[5] R.G. Keesee, A.W. Castleman, Jr., J. Phys. Chem. Ref. Data 15 (1986) 1011.
[6] E.E. Ferguson, N.G. Adams, D. Smith, Chem. Phys. Lett. 128 (1986) 84.
[7] J. Baker, A.D. Buckingham, J. Chem. Soc. Faraday Trans. 83 (1987) 1609.
[8] K. Luther, J. Troe, in A. Fontijn, M.A.A. Clyne (Eds.), Reaction of Small Transient Species, Academic, London, 1983.
[9] D.L. Albritton, in P. Ausloos (Ed.), Kinetics of Ion-Molecule Reactions, Plenum, New York, 1979.
[10] J. Glosík, V. Skalský, C. Praxmarer, D. Smith, W. Freysinger, W. Lindinger, J. Chem. Phys. 101 (1994) 3792.
[11] M. Tichy, G. Javahery, N.D. Twiddy, E.E. Ferguson, Int. J. Mass Spectrom. Ion Processes 93 (1989) 105.
[12] W. Lindinger, M. McFarland, F.C. Fehsenfeld, D.L. Albritton, A.L. Schmeltekopf, E.E. Ferguson, J. Chem. Phys. 63 (1975) 2175.
[13] H. Villinger, J.H. Futrell, A. Saxer, R. Richter, W. Lindinger, J. Chem. Phys. 80 (1986) 6995.
[14] J. Glosík, W. Freysinger, A. Hansel, P. Španěl, W. Lindinger, J. Chem. Phys. 98 (1993) 6995.
[15] J. Glosík, V. Skalský, W. Lindinger, Int. J. Mass Spec. Ion Processes 134 (1994) 67.
[16] H.W. Ellis, R.Y. Pai, E.W. McDaniel, E.A. Mason, L.A. Viehland, At. Data Nucl. Data Tables 17 (1976) 177.
[17] H.W. Ellis, E.W. McDaniel, D.L. Albritton, L.A. Viehland, S.L. Lin, E.A. Mason, At. Data Nucl. Data Tables 22 (1978) 179.
[18] N.G. Adams, D. Smith, Int. J. Mass Spectrom. Ion Processes 81 (1987) 273.
[19] J. Glosík, D. Smith, P. Španěl, W. Freysinger, W. Lindinger, Int. J. Mass Spectrom Ion Processes 129 (1993) 131.
[20] E.A. Gislason, E.E. Ferguson, J. Chem. Phys. 87 (1987) 6474.
[21] L. Pauling, The Nature of the Chemical Bond, 3rd ed., Cornell University Press, 1960.
[22] R.S. Mulliken, J. Am. Chem. Soc. 74 (1952) 811.
[23] M. McFarland, D.L. Albritton, F.C. Fehsenfeld, E.E. Ferguson, A.L. Schmeltekopf, J. Chem. Phys. 56 (1973) 6620.
[24] P.W. Atkins, Physical Chemistry, Oxford University Press, Oxford, 1988.
[25] E.B. Smith, Basic Chemical Thermodynamics, Clarendon, Oxford, 1982.
[26] K. Hiraoka, G. Nakajima, J. Chem. Phys. 88 (1988) 7709.